# Real-time observation of flexible domain movements in Cas9

Saki Osuka[1,2], Kazushi Isomura[1,2], Shohei Kajimoto[1], Tomotaka Komori[1], Hiroshi Nishimasu[1], Tomohiro Shima[1†], Osamu Nureki[1†], and Sotaro Uemura[1]

1, Department of Biological Sciences, Graduate School of Science, The University of Tokyo, 2-11-16 Yayoi, Bunkyo-ku, Tokyo 113-0032, Japan.

2, Authors contributed equally to this work.

†, Address correspondence to: Tomohiro Shima and Osamu Nureki,

Department of Biological Sciences, Graduate School of Science, The University of Tokyo, 2-11-16 Yayoi, Bunkyo-ku, Tokyo 113-0032, Japan

T.S Tel: +81-3-5841-4399; Fax: +81-3-5841-4397;

E-mail: tomohiro.shima@bs.s.u-tokyo.ac.jp

O.N. Tel: +81-3-5841-4392; Fax: +81-3-5841-8057;

E-mail: nureki@biochem.s.u-tokyo.ac.jp

Running title: Flexible domain movement in Cas9

## ABSTRACT

**The CRISPR-associated protein Cas9 is a widely used genome editing tool that recognizes and cleaves target DNA through the assistance of a single-guide RNA (sgRNA). Structural studies have demonstrated the multi-domain architecture of Cas9 and sequential domain movements upon binding to sgRNA and the target DNA. These studies also have hinted at flexibility between the domains, but whether these flexible movements take place under dynamic and physiological conditions is unclear. Here, we directly observed dynamic fluctuations by multiple Cas9 domains using single-molecule FRET. The flexible domain movements allow Cas9 to take transient conformations beyond those revealed by crystal structures. Importantly, one Cas9 nuclease domain accessed to the DNA cleavage position only during such flexible movement, suggesting the importance of this flexibility in the DNA cleavage process. Moreover, changes in domain flexibility in the presence of nucleic acids indicated that flexible Cas9 domain movements are involved in the sgRNA and the target DNA binding processes. Collectively, our results highlight the potential role of fluctuations in driving Cas9 catalytic processes.**

**Key words**

Fluctuations, Gene-editing, Intramolecular FRET, Conformational plasticity

## INTRODUCTION

CRISPR (Clustered regularly interspaced short palindromic repeats)-Cas (CRISPR-associated) systems were originally found as natural genome defense systems that possessed adaptive immunity against virus and plasmid in bacteria and archaea (Jansen *et al*, 2002; Mojica *et al*, 2005; Bolotin *et al*, 2005; Pourcel *et al*, 2005; Barrangou *et al*, 2007). Unlike other CRISPR-Cas systems that employ ensembles of Cas proteins to recognize and cleave nucleic acids, the type II CRISPR-Cas system utilizes only one endonuclease, Cas9, to recognize and cleave target DNA (Shmakov *et al*, 2017). *Streptococcus pyogenes* Cas9 (henceforth, Cas9) has been widely used as a powerful genome editing tool ( Mali *et al*, 2013; Cong *et al*, 2013), especially since the first demonstration that Cas9 can be programmed by synthetic single guide RNA (sgRNA) to cleave any specific DNA sequences that are followed by a protospacer-adjacent motif (PAM) sequence (Jinek *et al*, 2012). In addition, Cas9 has been applied to visualize, modify and express endogenous target genes (Hsu *et al*, 2014; Sternberg & Doudna, 2015; Terns & Terns, 2014; Konermann *et al*, 2014). The continuously expanding application of Cas9 technologies has stimulated a strong interest in the molecular basis of how Cas9 recognizes and cleaves DNA.

Already, a series of Cas9 crystal structures with and without the sgRNA and target DNA has been solved (Jinek *et al*, 2014; Nishimasu *et al*, 2014; Jiang *et al*, 2016, 2015; Anders *et al*, 2014). These structural studies demonstrate the multi-domain architecture of Cas9, which mainly consists of a recognition (REC) lobe and a nuclease lobe. The nuclease lobe can be further divided into the HNH, RuvC and PAM-interacting (PI) domains. The crystal structures also revealed sequential rearrangements of the Cas9 domains upon binding to the sgRNA and target DNA. The binding of sgRNA induces a large rotation of the nuclease lobe to convert Cas9 into the active conformation with a

central channel, which can accommodate the target DNA. The PI domain recognizes the PAM sequence in the target DNA, leading to the guide:target heteroduplex formation by sgRNA with the complementary strand of the target DNA in the REC lobe (Nishimasu *et al*, 2014; Jiang *et al*, 2016; Anders *et al*, 2014). DNA binding induces translocation of the HNH domain and conformational changes in the RuvC domains to cleave the two strands of the target DNA. These domain rearrangements during Cas9 catalytic processes have been further confirmed by bulk FRET measurements (Sternberg *et al*, 2015).

The above structural studies have revealed the distinct Cas9 domain configurations of the apo, sgRNA-bound and sgRNA/DNA-bound states. However, conformational plasticity and flexibility of Cas9 has been predicted, and additional crystal structures have shown some disordered motifs/domains, suggesting that the domain configurations are flexible in specific conditions (Nishimasu *et al*, 2014; Jiang *et al*, 2016). Based on crystal structures and bulk FRET measurements, the HNH domain in the sgRNA/DNA-Cas9 ternary complex, in particular, has been predicted to take at least two distinct positions relative to the REC lobe: the DNA-docked position and the DNA-undocked position (Nishimasu *et al*, 2014; Jiang *et al*, 2016; Sternberg *et al*, 2015). The transition of the HNH domain from the undocked to docked position is crucial for DNA cleavage, because the active site in the undocked HNH domain locates approximately 30 Å away from the cleavage sites in the complementary DNA strand (Nishimasu *et al*, 2014). Additively, mismatch base pairs in the guide:target heteroduplex hampers the HNH transition (Sternberg *et al*, 2015), suggesting that flexibility of the HNH domain is closely related with not only DNA cleavage but also DNA recognition. A previous single molecule study has implied conformational flexibility during the DNA binding process (Singh *et al*, 2016) and molecular dynamics

simulations also have shed light on the importance of flexible movements of the Cas9 domain in the sgRNA/DNA binding and recognition (Zheng, 2017). Thus, flexibility in the Cas9 domain configuration could be an important factor in Cas9 catalytic processes.

Insight on this possibility would be gained from direct experimental evidence of the flexible movements of the Cas9 domains in dynamic and physiological conditions. These conditions could clarify whether the Cas9 domains are flexible even in steady state in the presence or absence of nucleic acids. To address this question, we directly observed the movement between the REC lobe-RuvC, REC lobe-HNH and HNH-RuvC domains using single molecule FRET (smFRET) by labeling the domains with different fluorescent dyes. A subset of Cas9 molecules demonstrated dynamic fluctuations in FRET efficiency, providing strong evidence that the Cas9 domains move in a flexible and reversible manner. Moreover, our measurements revealed the flexible domain movements are dependent on nucleic acids and cations, yielding new insights into the molecular basis of the Cas9 catalytic process.

## RESULTS

### Experimental setup for single molecule FRET measurements of Cas9.

To directly observe the flexibility of the Cas9 domains at the single molecular level, Cas9 was site-specifically labeled with Cy3 and Cy5 fluorochromes. Using C80L/C574E cysteine-free Cas9, which has activity comparable to wild-type Cas9 (Nishimasu *et al*, 2014), as a starting construct, we introduced three pairs of cysteine residues at D435/E945, S355/S867 and S867/N1054 in Cas9, as done in a previous bulk FRET study (Sternberg *et al*, 2015). These three FRET constructs were designed to monitor the movements between REC lobe-RuvC (D435C-E945C), REC lobe-HNH (S355C-S867C) and HNH-RuvC (S867C-N1054C), respectively (Figure 1A-C). The introduced cysteine residues were labeled with Cy3- (donor) and Cy5- (acceptor) maleimide. Further, the constructs were genetically fused with biotin-carboxyl-carrier-protein (BCCP) at their N-terminus to anchor the Cas9 molecules on the glass surface via avidin-biotin linkage (Figure 1D). We first examined whether the FRET constructs retain catalytic activity. All three BCCP-tagged fluorescent Cas9 constructs showed over 90% DNA cleavage activity compared with wild-type Cas9 (Figure EV1), confirming that the Cas9 activity is not substantially affected by the fluorescent labeling and fusion with the BCCP-tag.

We then performed smFRET measurements of the fluorescent Cas9 molecules in nucleic-acid free, sgRNA-bound and sgRNA/DNA-bound conditions under total internal reflection fluorescent microscopy (TIRFM). To ensure the binding states of the Cas9 molecules in each condition, we incubated 0.3 to 1 nM fluorescent Cas9 and 200 nM sgRNA with or without 200 nM target DNA for measurements of the sgRNA-bound and sgRNA/DNA-bound Cas9 molecules. Considering the saturation rate of sgRNA on Cas9 (Figure EV2) and the dissociation constants value ($K_d$) of 0.8 nM for the target

DNA loading into sgRNA-bound Cas9 (Sternberg *et al*, 2015), we assumed that almost all fluorescent Cas9 molecules were occupied with nucleic acids under our assay conditions. The sgRNA/DNA-bound molecules in our assay should maintain the ternary complex of the sgRNA and cleaved target DNA, because previous studies have demonstrated that Cas9 cleaves the target DNA at a rate higher than 10 $min^{-1}$ and retains binding with cleaved DNA (Sternberg *et al*, 2014; Jinek *et al*, 2012; Sternberg *et al*, 2015). The Cas9 molecules were then anchored on the glass surface through BCCP and illuminated with a 532-nm laser under TIRFM. The FRET efficiency of each Cas9 molecule was calculated from the recoded fluorescence intensity of Cy3 and Cy5 (Figure 1E). After the smFRET measurements, we confirmed that the majority of observed Cas9 molecules labeled with Cy3 and Cy5 showed FRET under any tested condition (Table EV1) using the acceptor bleaching method (see Method Details). Thus, we further analyzed the FRET trajectories of Cas9 molecules that showed FRET.

**Dynamic rearrangements of Cas9 domains upon nucleic acids binding**

From the FRET efficiency of the Cas9 molecules (Figure 2), we validated the dynamic rearrangements of the Cas9 domains upon sgRNA and target DNA bindings. The FRET efficiency of the labeled D435C-E945C construct decreased upon sgRNA binding (Figure 2A), supporting the model in which this binding turns the REC lobe against the RuvC domain. The S355C-S867C construct exhibited a gradual increase in FRET efficiency with binding of the sgRNA and then the target DNA (Figure 2B), suggesting the HNH domain approached the DNA-docked position stepwise with nucleic acid binding. This model of the HNH domain transition was further supported by our findings that the S867C-N1054C construct exhibited a gradual decrease upon sgRNA and target DNA binding (Figure 2C). Note that changes in the both distance and

orientation between the domains would contribute to the FRET efficiency shifts because the fluorochromes on the Cas9 molecules showed high anisotropy (0.23-0.33 for Cy3 and 0.20-0.28 for Cy5, see Method Details). However, the timing and direction of the shifts were completely consistent with the previously proposed Cas9 domain rearrangement model (Nishimasu *et al*, 2014; Jinek *et al*, 2014; Jiang *et al*, 2015, 2016).

**Cas9 domains showed highly flexible and reversible movements**

Although the overall shifts in the mean FRET efficiency were consistent with the domain rearrangement model (Nishimasu *et al*, 2014; Sternberg *et al*, 2015; Jinek *et al*, 2014; Jiang *et al*, 2015, 2016), our measurements also demonstrated that individual Cas9 molecules can take different domain configurations than those observed in crystal structures. The histograms of the FRET efficiency under all the tested conditions did not exhibit simple one-peak distributions (Figure 2), suggesting that the distances and/or angles between the Cas9 domains are not fixed under nucleic acid binding conditions. Accordingly, the observed wide distribution of the FRET efficiency may reflect the flexible nature of the Cas9 domains. Consistent with this idea, a fraction of Cas9 molecules showed frequent fluctuations in FRET efficiency between multiple FRET states (Figure 3). These fluctuations indicate highly flexible and reversible movements of the Cas9 domains and mark the first direct observation of Cas9 domain fluctuations in dynamic and physiological conditions.

The percentage of molecules showing FRET efficiency fluctuations changed depending on the binding state of Cas9 (Figure 3). When we observed for long periods of time, some molecules exhibited transitions between the very static state and the highly fluctuating state (Figure 3C), suggesting that the Cas9 domains are in equilibrium between the static and fluctuating states. Since flexibility of the Cas9

domains should affect this equilibrium, we considered the percentage of fluctuating molecules as an indicator of domain flexibility. Here, we defined a fluctuating molecule as a fluorescent-labeled Cas9 that showed more than two anti-correlated shifts in the fluorescence intensity of Cy3 and Cy5 during our observation period. As a common property of the D435C-E945C and S355C-S867C constructs, sgRNA binding decreased the percentage (Figure 2B), suggesting that the flexibility between the REC lobe and the nuclease lobe (HNH and RuvC domains) are stabilized by sgRNA binding. The high flexibility between the lobes in apo-Cas9 could allow Cas9 to take a transient conformation that may provide an active sgRNA binding interface, possibly increasing the efficiency of binding with sgRNA. To support this idea, we found that the FRET efficiency of fluctuating D435C-E945C molecules in the apo state was widely distributed from 0 to 1, contrary to the very narrow FRET distribution of static molecules in the apo state (Figure EV3). Considering the widespread FRET distribution of sgRNA-bound D435C-E945C (Figure EV3A), we concluded some of the fluctuating molecules in the apo state take a conformation that resembles the sgRNA-bound active form of Cas9. In contrast to the sgRNA binding, the target DNA binding increased the percentage of fluctuating molecules of both constructs (Figure 3D). The increased percentage suggests increased flexibility in the hinge region between the REC and nuclease lobes in the sgRNA/DNA-Cas9 ternary complex.

As for S867C-N1054C, among the three nucleic acid binding states, the construct with sgRNA exhibited the highest percentage of fluctuating molecules (Figure 3D), suggesting that the binding of sgRNA destabilizes the link between the HNH and RuvC nuclease domains but the following target DNA binding stabilizes it. Similar to the other constructs, the FRET state distribution of static and fluctuating S867C-N1054C molecules were different (Figure EV3). The FRET distribution of the static molecules

showed a narrow peak at high FRET efficiency in the apo state and gradual appearance of a low FRET population upon sgRNA and DNA bindings. In contrast, the fluctuating molecules frequently showed low FRET efficiency already in the apo and sgRNA-bound states. These results support the idea that flexible domain movements assist Cas9 to take a conformation resembling the static conformation of the following nucleic acid binding states. Compared with the other two constructs, S867C-N1054C showed relatively low fluctuating molecules (Figure 3D); however, there is a possibility that we underestimated the fluctuating molecules because, due to the short distance between S867 and N1054 residues (Nishimasu *et al*, 2014), the construct requires a relatively larger domain displacement for the FRET efficiency shift. Thus, it is not appropriate to compare the flexibility of these three domains observed in the three constructs. Yet, because the percentage of fluctuating molecules of all three constructs highly depended on the binding state of Cas9, we conclude that the nucleic acids bindings regulate the flexibility of these three Cas9 domains.

**The HNH domain accessed to the DNA-cleavage position only during the flexible movement**

To access the effects of the flexible domain movements on the DNA cleavage process, we further analyzed the movements of the HNH nuclease domain in the sgRNA/DNA-Cas9 ternary complex. The distribution of FRET efficiency of the fluctuating S355C-S867C molecules in the ternary complex exhibited several clear peaks, contrary to the widespread distribution of the apo-Cas9 and sgRNA-bound binary complex (Figure 4). These results suggest that the HNH domain in the ternary complex moves between distinct positions relative to the REC lobe and the REC lobe-bound target DNA strand. Consistently, previous studies have demonstrated that the ternary

complex can take two conformations in which the HNH domain is docked or undocked at the cleavage site of the target strand (Nishimasu *et al*, 2014; Jiang *et al*, 2016). Since Cas9 require magnesium ions for DNA cleavage (Jinek *et al*, 2012), in the absence of magnesium ions Cas9 can be trapped in the pre-cleavage state with sgRNA and DNA. In the absence of magnesium ions, the peak values of the FRET efficiency were ~0.2 and ~0.8. The lower FRET efficiency indicates the longer distance between the HNH domain and the cleavage site; hence, we considered molecules with lower FRET efficiency as representing the HNH-undocked conformation and those with higher FRET efficiency as representing the HNH-docked conformation. Although the ratio of fluctuating molecules in this condition was comparably low (mean ± SEM. = 7 ± 1 %) with that of the Cas9-sgRNA binary complex, the time trajectories of the FRET efficiency suggest that the HNH domain in the ternary complex fluctuates among the docked and undocked positions even in the pre-cleavage state.

The addition of magnesium ion to the ternary complex clearly changed the manner of the HNH fluctuations (Figure 4A). The addition of magnesium ion enhances the percentage of fluctuating molecules more than two-fold (Figure 3D). Such fluctuating sgRNA/DNA-bound S355C-S867C molecules showed three major peaks in their FRET efficiency (approximately 0.4, 0.8 and 1.0). The time trajectories of the FRET efficiency demonstrated frequent and reversible transitions between these three FRET states (Figure 5A). The highest FRET efficiency, which was not observed under magnesium-free condition, suggests that the HNH domain can locate this third position to the target DNA only in the presence of magnesium ion. Because magnesium ion also initiated DNA cleavage, this third position would represent the state from which the HNH domain cleaves the target DNA. Consistently, the highest FRET efficiency represents a very short distance between the active site of the HNH domain and the

cleavage site of the complementary DNA strand. Therefore, we name this HNH position corresponding to the highest FRET efficiency the DNA-cleavage position. Just as under the magnesium-free condition, the ternary complex can also take the conformation corresponding to the FRET efficiency value of ~0.8. Considering the inability of Cas9 without magnesium ion to cleave DNA, we name the HNH position in this conformation as the pre-cleavage position. Our measurements suggest that the HNH domain fluctuates between these two distinct positions in the HNH-docked conformation and the undocked position. Because very few Cas9 molecules in the static state showed the FRET efficiency that corresponds to the DNA-cleavage HNH position (Figure 4B), the flexible movement would be critical for the HNH domain to locate at the DNA-cleavage position and therefore very important for the nuclease process of Cas9.

Finally, we further investigated the movements of the HNH domain among the three positions. To analyze the relationship of the positions before and after transitions of the HNH domain in the ternary complex, we measured the FRET time trajectories of sgRNA/DNA-bound S355C-S867C using a hidden Markov model-based algorithm (Figure 5A) and plotted the FRET efficiency of the pre- and post-HNH transitions (Figure 5B). Together with the transition density plot and Silhouettes analysis (Figure EV4), the transition can be classified into five types: transitions from a low FRET state to another low FRET state, between low and middle FRET states in both directions and between low and high FRET states in both directions. To our surprise, transitions between middle and high FRET states were rare (less than 2% of the all transitions), suggesting that the docked HNH domain rarely moves between the pre-cleavage and DNA-cleavage positions and therefore needs to take the undocked conformation before relocating to another docked position.

Among the five types, transitions from the high FRET state showed the longest duration before transition (Figure 5C), suggesting high stability of the HNH domain in the DNA-cleavage position compared to that in other positions. On the contrary, durations before all three types of transitions from the low FRET state (low-low, low-middle and low-high FRET state transitions) were approximately half that of the high-to-low FRET state transition. The results indicate that the HNH domain in the undocked conformation frequently changes its position. The flexible movement of the undocked HNH domain was also demonstrated in the scattered plots of the low FRET state in the transition density map. This frequent and flexible movement of the undocked HNH domain may facilitate HNH translocation to the DNA-cleavage position and the DNA-cleavage process.

## DISCUSSION

The purpose of the present study is to investigate whether Cas9 has a flexible structure as predicted by previous studies (Nishimasu *et al*, 2014; Sternberg *et al*, 2015; Singh *et al*, 2016; Zheng, 2017; Jiang *et al*, 2016). Here, using the smFRET technique, we directly observed the dynamic fluctuations of the Cas9 domains. These fluctuations allow Cas9 to take different conformations besides those previously reported by crystal structures (Nishimasu *et al*, 2014; Jiang *et al*, 2016). Our detailed analysis highlights the potential roles of transient conformations regulated by the flexibility in both the DNA cleavage and the sgRNA/DNA binding processes.

Here, we summarize the flexibility of Cas9 domain configuration observed in the present study (Figure 6). Judging from the population of the fluctuated molecules (Figure 3D), the HNH domain together with the RuvC domain flexibly moved relative to the REC lobe in the apo-Cas9. The binding of sgRNA stabilizes the fluctuations

between the nuclease domains and the REC lobe, but enhances the fluctuations between the HNH and RuvC domains. Conversely, the following target DNA binding enhances the fluctuations between the nuclease domains and the REC lobe, but stabilizes the fluctuations between the HNH and RuvC domains (Figure 3D).

In the cleavage process of target DNA, flexible movement of the HNH nuclease domain would be critically important. When we monitored the relative position of the HNH domain to the REC lobe using the S355C-S867C construct, the HNH domain in the ternary complex with magnesium ion fluctuated between three distinct positions: undocked, pre-cleavage and DNA-cleavage positions (Figure 5). The HNH domain in the DNA-cleavage position would be directly related to the Cas9 nuclease activity, because the HNH domain in the same construct without magnesium ion, which is unable to cleave DNA, could not access the position (Figure 4A). Furthermore, even in the presence of magnesium ion, the construct in the static phase did not show the high FRET efficiency corresponding the DNA-cleavage HNH position (Figure 4B). Our results showing that the HNH domain can access to the DNA-cleavage position only during the fluctuation phase emphasize the importance of flexible movement of the HNH domain in the DNA cleavage process. Besides its direct participation in the cleavage process of the complementary DNA strand, the HNH flexibility may also affect the cleavage of the noncomplementary strand through interaction with the RuvC domain. Consistent with this idea, movement of the HNH has been reported to control the nuclease activity of the RuvC domain on the noncomplementary DNA strand through intramolecular communication between the two domains (Sternberg *et al*, 2015; Jiang *et al*, 2016). In contrast to the relation of the HNH and the REC lobe, fluctuation between the HNH and RuvC domain was stabilized by the binding of the target DNA. The stable interaction of the HNH and RuvC domains in the ternary complex may

contribute to the intramolecular communication, and thus to the DNA cleavage of both strands. Together, our results underscore the importance of the flexible movements of the HNH domain in Cas9 nuclease activity.

In addition to the DNA cleavage process, the sgRNA and target DNA binding processes of Cas9 can be affected by the domain fluctuations. To explain, first we focus on the process of the sgRNA binding. Structural studies have demonstrated that apo-Cas9 takes an autoinhibited conformation in which active sites in the HNH and RuvC domains locate away from the DNA binding cleft (Jinek *et al*, 2014). In this form, possible interaction interfaces with the sgRNA are limited. Highly flexible movements by both domains relative to the REC lobe (Figure 3D) may turn the active sites towards the DNA binding cleft, as predicted by molecular dynamics simulations (Zheng, 2017), and provide additional transient interaction interfaces. Consistently, unlike static molecules, some of the fluctuating apo-Cas9 molecules we observed showed FRET efficiency resembling that of sgRNA-bound Cas9 (Figure EV3). The results can be well explained by the transient rotation of the REC lobe to the nuclease domains in the apo-Cas9. Therefore, the flexible movements of the REC lobe may transiently change apo-Cas9 into an active form and promote binding of the Cas9 to the sgRNA. Similarly, the fluctuating sgRNA-bound Cas9 frequently showed the similar FRET efficiency to that of the static sgRNA/DNA-bound Cas9, raising the possibility that the domain flexibility involved also in the binding of the target DNA.

Although verification of the function of the flexible movements awaits further studies, our results open a new door to modify and expand Cas9-based tools by modulating the domain flexibility. The flexibility shown here is likely to assist transient formation of additional interaction interfaces of Cas9 and the sgRNA/DNA. Recent mutagenesis studies have emphasized the importance of controlling a number of

non-specific DNA contacts on the off-target DNA binding ability (Slaymaker *et al*, 2016; Kleinstiver *et al*, 2016). Thus, modulation of the flexibility may change Cas9 tolerance for sgRNA/DNA sequence variation. Moreover, our detailed analysis demonstrated that the HNH flexible movement between the pre-cleavage and the DNA-cleavage position is very rare, suggesting that the HNH domain in the pre-cleavage position is required to return to the undocked position before it translocates to the DNA-cleavage position. Therefore, mutations in the interface of the HNH domain and the REC lobe that destabilize the HNH domain in the pre-cleavage position may facilitate HNH translocation to the DNA-cleavage position for faster DNA cleavage by Cas9. Collectively, our data could provide useful information for future improvements in Cas9-based tools for gene-editing, gene-visualizing and gene expression control.

## MATERIALS AND METHODS

### Sample Preparation

Since Cas9 C80L/C574E mutations do not affect the cleavage activity and improve the solution behavior of Cas9 (Nishimasu *et al*, 2014), we used the Cas9 C80L/C574E mutant as wild-type Cas9 in this study. We introduced the mutations into the Cas9 C80L/C574E mutant to prepare D435C-E945C, S355C-S867C and S867C-N1054C. The Cas9 proteins were prepared as previously described (Nishimasu *et al*, 2014), with minor modifications. Briefly, the Cas9 variants were expressed as $His_6$-GST-fusion proteins at 20°C in *Escherichia coli* Rosetta 2 (DE3) (Novagen) and purified by chromatography on Ni-NTA Super flow resin (QIAGEN). The $His_6$-GST tag was removed by TEV protease digestion, and the proteins were further purified by chromatography on Ni-NTA, HiTrap SP HP (GE Healthcare), and Superdex 200 Increase (GE Healthcare) columns. The purified Cas9 was stored at −80 °C until use.

### *In Vitro* Cleavage Assay

*In vitro* cleavage experiments were performed as previously described (Anders et al., 2014), with minor modifications. A *Eco*RI-linearized pUC119 plasmid (100 ng, 5 nM) containing the 20-nt target sequence and the NGG PAM was incubated at 37°C for 5 min with the Cas9–sgRNA complex (25 and 50 nM) in 10 μL of reaction buffer containing 20 mM HEPES-NaOH, pH 7.5, 100 mM KCl, 2 mM $MgCl_2$, 1 mM DTT, and 5% glycerol. The reaction was stopped by the addition of a solution containing EDTA (40 mM final concentration) and Proteinase K (1 mg/mL). Reaction products were resolved on an ethidium bromide-stained 1% agarose gel and then visualized using an Amersham Imager 600(GE Healthcare).

**Preparation of single-guide RNA and a target plasmid DNA**

The sgRNA was transcribed *in vitro* with T7 RNA polymerase using a PCR-amplified DNA template and purified by 10% denaturing (7M urea) PAGE. Target plasmid DNA was amplified in *E.* coli DH5a strain in LB medium (Nacalai Tesque, Inc., Japan) at 37°C overnight. Plasmid DNA was purified using a Midiprep kit (FastGene Xpress Plasmid PLUS Kit, NIPPON Genetics) according to the provider's method. The concentration of purified plasmid DNA was determined based on the absorption at 260 nm using NanoDrop 2000c (Thermo Fisher). The single-guide RNA and plasmid DNA were stored at −80°C and −30°C until use, respectively.

**Fluorescent labeling of Cas9**

Cas9 was fluorescently labeled using Cy3- and Cy5-maleimide (GE healthcare) according to a general method. Briefly, the buffer for Cas9 was exchanged into the labeling buffer (20 mM HEPES-KOH pH 7.0, 100 mM KCl, 2 mM $MgCl_2$, 5% glycerol) using a spin-gel filtration column (Micro Bio-Spin 30, BioRad). Next, Cas9 solution was incubated on ice for 30 min after final 0.5 mM TCEP addition into the Cas9 solution. Then, Cy3- and Cy5 maleimide were mixed with Cas9 solution at the molar ratio between protein and each dye of 1: 20. The maleimide labeling reaction was conducted on ice for 2 h. Excessive fluorescent dye maleimide was removed twice using assay buffer (AB: 20 mM HEPES-KOH pH7.5, 100 mM KCl, 2 mM $MgCl_2$, 5% glycerol, 0.5 mM EDTA, 1 mM DTT) and spin-gel filtration columns (Micro Bio-Spin 30, BioRad). The fluorescent Cas9 was snap-frozen in liquid nitrogen and stored at −80 °C until use.

**Fluorescence spectrometer FRET measurement for stoichiometry of sgRNA binding to Cas9.**

All fluorescence measurements used a reaction mixture of 20 nM fluorescent Cas9 (D435C-E945C) with or without sgRNA (10 nM, 20 nM, 50 nM, 100 nM or 200 nM) in AB with 0.1 U/μL RNasin Plus (Promega) and a commercial oxygen scavenger system (Pacific Bioscience) containing 2.5 mM TSY, 2.5 mM protocatechuic acid (PCA) and 50 times diluted protocatechuic acid dehydrogenase (PCD) solution and were performed using a fluorescence spectrometer (RE-6000, Shimazu, Japan), quartz cuvette of 50 μL volume (T-703M-ES-10.50B, TOSOH, Japan), 532 nm excitation and scanning speed of 60 nm/min at a wavelength range of 550 nm to 750 nm in 1 nm increments at room temperature.

**Perrin plot to determine the orientation factors.**

All fluorescence measurements using the reaction mixture of 100 nM fluorescent Cas9 (D435C-E945C, S355C-S867C and S867C-N1054C with no nucleic acid) in buffer (20 mM HEPES-KOH pH7.5, 100 mM KCl, 2 mM $MgCl_2$, 0.5 mM EDTA, 1 mM DTT and a commercial oxygen scavenger system) with or without methyl cellulose (0.001%, 0.01%, 0.1% or 1%) were performed at room temperature using the same fluorescence spectrometer and cuvette described in the above section. The orientation factor $\kappa^2$ was determined as described below according to the previous method (Dale *et al*, 1979). Briefly, the fluorescence anisotropy measurement was performed by manually placing the polarization filters in front of the exciter and detector in the fluorescence spectrometer. For Cy3, the fluorescence intensity was measured at a wavelength of 566 nm by 554 nm excitation, while that of Cy5 was measured at a wavelength of 668 nm by 650 nm excitation. The slit width for emission and excitation was 5 nm, and the

integration time was 1 s. Each measurement was repeated three times. Using these fluorescence intensities, fluorescence anisotropy $r$ was calculated as below.

$$r = (Ivv - G)/(Ivv + 2G)$$

$$G = Ihv\,\frac{Ivh}{Ihh}$$

*Ivh* indicates the fluorescence intensity of the horizontal polarization excited by vertical polarized light. *Ivv*, *Ihv* and *Ihh* are defined similarly. Following the plotting of $1/r$ against $T/\eta$, the y-intercept was calculated by fitting the plot to the linear function for each fluorescent Cas9 ($T$: absolute temperature and $\eta$: viscosity of the sample). Here, $\eta$ was 0.89, 1.64, 8.39, 75.89 and 750.89, which corresponds to 0, 0.001, 0.01, 0.1 and 1% methyl cellulose solution, respectively. In the case of low anisotropy, $\kappa^2$ is close to the dynamic isotropic limit of $\kappa^2 = 2/3$. Otherwise, $\kappa^2$ widely distributes in the range of $0 \leq \kappa^2 \leq 4$. Thus, the high anisotropy of Cy3 and Cy5 obtained, which is close to the theoretical maximum value of 0.4, obscured the value of $\kappa^2$ so that we were unable to estimate distances between the two fluorochromes from the FRET efficiency.

**Single molecule FRET measurement of fluorescent Cas9**

A 0.5 μL volume micro-chamber was made by placing a polyethylene glycol (PEG) and biotinylated PEG coated small coverslip of 11 mm × 11 mm, which was cut from a commercial coverslip, over a larger one (22 mm × 22 mm, No.1S Thickness, Matsunami, Japan) and double-sided adhesive tape (30 μm thickness, NITTO DENKO, Japan) in a clean hood (Matsusada Precision Inc., Japan). First, 1 mg/mL Neutralized avidin (Wako, Japan) in AB was adsorbed on the glass surface. After 2 min incubation, excessive neutralized avidin was removed by 3 times 2 μL AB wash. Next, the glass

surface in the micro-chamber was illuminated by a 532 nm laser for 40 s per one field using fluorescence microscopy to photobleach any residual fluorescent particles on the glass surface. After 3 times 2 μL AB wash, 0.3 - 1 nM fluorescent Cas9 was adsorbed on the glass surface using avidin-biotin interaction. Here, for sgRNA-bound fluorescent Cas9 imaging, fluorescent Cas9 was incubated with final 200 nM sgRNA for 2 min at room temperature in a 0.6 mL tube before the Cas9 absorption, while fluorescent Cas9 was successively incubated with 200 nM sgRNA and 200 nM plasmid DNA for 2 min for sgRNA- and DNA-bound fluorescent Cas9 imaging. Followed by 2 min incubation and 3 times 2 μL AB wash, AB with a commercial oxygen scavenger system (Pacific Bioscience) containing 2.5 mM TSY, 2.5 mM protocatechuic acid (PCA) and 50 times diluted protocatechuic acid dehydrogenase (PCD) solution for all samples, 200 nM sgRNA for sgRNA-bound fluorescent Cas9 imaging and 200 nM sgRNA and 200 nM plasmid DNA for sgRNA- and DNA-bound Cas9 imaging. Finally, the micro-chamber was placed in total internal reflection fluorescence microscopy (TIRFM) for the single molecule FRET (smFRET) measurements.

The smFRET measurements of fluorescent Cas9 were achieved using Nikon Ti-E based TIRFM equipped with a multi-band filter set for fluorescence microscopy (LF405/488/532/635-A, Semrock), a dual-view apparatus (Optical Insights) containing a dichroic (630, Optical Insights) and emission filters (FF01-593/40-25 for Cy3 imaging and FF01-692/40-25 for Cy5 imaging, Semrock), and a back-illuminated EMCCD camera (Andor, iXon+). Illumination was provided by a 532 nm laser (Coherent, Sapphire) and 642 nm laser (Coherent, Cube). Image acquisition for the smFRET measurements were performed with the acquisition rate of 10 frames per second using 532 nm illumination and open source microscopy software (Micro-Manager, Open Imaging). The FRET efficiency distributions were calculated over the duration of

photobleaching of the fluorescent dye (donor or acceptor) or the entire observation time (120 s for D435C-E945C and S355C-S867C; 40 s for S867C-N1054C) in the case that no photobleaching was observed. Following the smFRET measurements, the same field was illuminated using a 642 nm laser to directly excite Cy5 fluorescence for the counting of Cy3 and Cy5 double-labeled Cas9 and to confirm whether the Cy5 fluorescence intensity decrease was caused by fluorescence photobleaching.

For the smFRET analysis, the exported image data were imported into a home built program written in Python and converted into fluorescence intensity based on the fluorescent spots of both Cy3- and Cy5-labeled Cas9. The FRET efficiency of a single molecule was calculated as $I_A/(I_A+\gamma I_D)$ (Roy *et al*, 2008). Here, $I_A$ and $I_D$ are the fluorescence intensity of the acceptor and donor, respectively. $\gamma$ is equivalent to $|\Delta I_A/\Delta I_D|$, where $\Delta I_A$ and $\Delta I_D$ are the fluorescence intensity change of the acceptor and donor upon FRET efficiency fluctuation or photobleaching, respectively. The transition points in the fluctuating traces of sgRNA/DNA-bound fluorescent Cas9 (S355C-S867C) were detected based on the Hidden Markov Model (HMM) with the Baum-Welch forward-backward algorithm and Viterbi algorithm (McKinney *et al*, 2006) using the hmmlearn library for Python (https://github.com/hmmlearn/hmmlearn). Here, we assumed that HMM has three states according to the FRET efficiency distribution (the bottom histogram in Figure 4A). The transition density plot was visualized using a Python plotting library (Matplotlib; http://matplotlib.org), while the plotted density was clustered into five groups based on the k-means method with $k$ = 5 using the machine learning package for Python (Scikit-learn; http://scikit-learn.org/).

## ACKNOWLEDGEMENTS

This study is supported by JST, CREST, JPMJCR14W1 (to S.U) and MEXT, Grant-in-Aid for Young Scientists (B), 15K18514 (to T.S.). We thank members of the Uemura and Nureki laboratories for valuable discussion. We also thank M.Sugawa for technical help and P. Karagiannis for helpful discussions and comments on the manuscript.

**Author contributions**

T.K., H.N., T.S., O.N. and S.U. designed the study. S.O. collected and analyzed smFRET data; K.I. and T.K. collected and analyzed bulk FRET data; K.I. and S.K. prepared the fluorescent-labeled protein and performed functional analysis; S.K., T.K., H.N., T.S., O.N. and S.U. wrote the paper. All authors discussed the results and commented on the manuscript.

**Conflict of interest**

The authors declare no conflict of interest.

**Figure Legends**

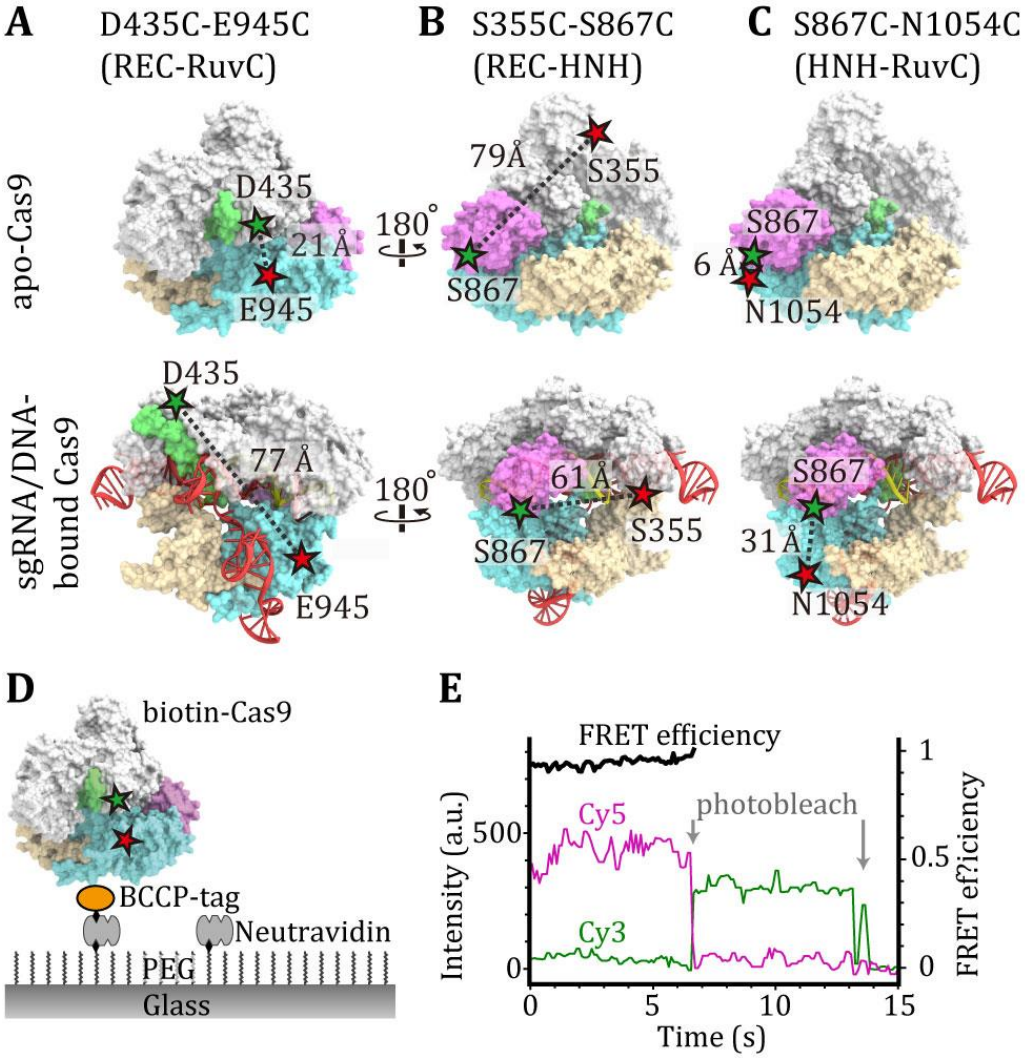


**Figure 1. Experimental setup for smFRET measurement of Cas9 domain movements.**

(A-C) Designs of Cas9 for single molecule FRET (smFRET) measurements. We constructed three constructs: D435C-E945C (A), S355C-S867C (B) and S867C-N1054C (C). Surface rendered models of Cas9 were generated from PDB 4CMP for apo-Cas9 (upper models) and PDB 4OO8 for sgRNA/DNA-bound Cas9 (bottom models). HNH-domain, REC lobe, RuvC domain, PI domain, Bridge helix, sgRNA and

target DNA are colored pink, gray, blue, light brown, green, red and yellow, respectively. The labeled amino acids are described using green and red stars. (D) Schematic drawing of the smFRET measurement system. Biotinylated Cas9 via BCCP (Biotin Carboxyl Carrier Protein) was immobilized on a PEG (polyethylene glycol)- and biotin-PEG-coated glass surface using the avidin-biotin system. Images are not to scale. (E) Time trajectories of single-molecule FRET efficiency of the D435C-E945C construct labeled with Cy3 and Cy5. The green and magenta lines represent the fluorescence intensity of Cy3 and Cy5, respectively. We calculated the FRET efficiency (black lines) from the intensity of Cy3 and Cy5 before the photobleaching of either fluorochrome.

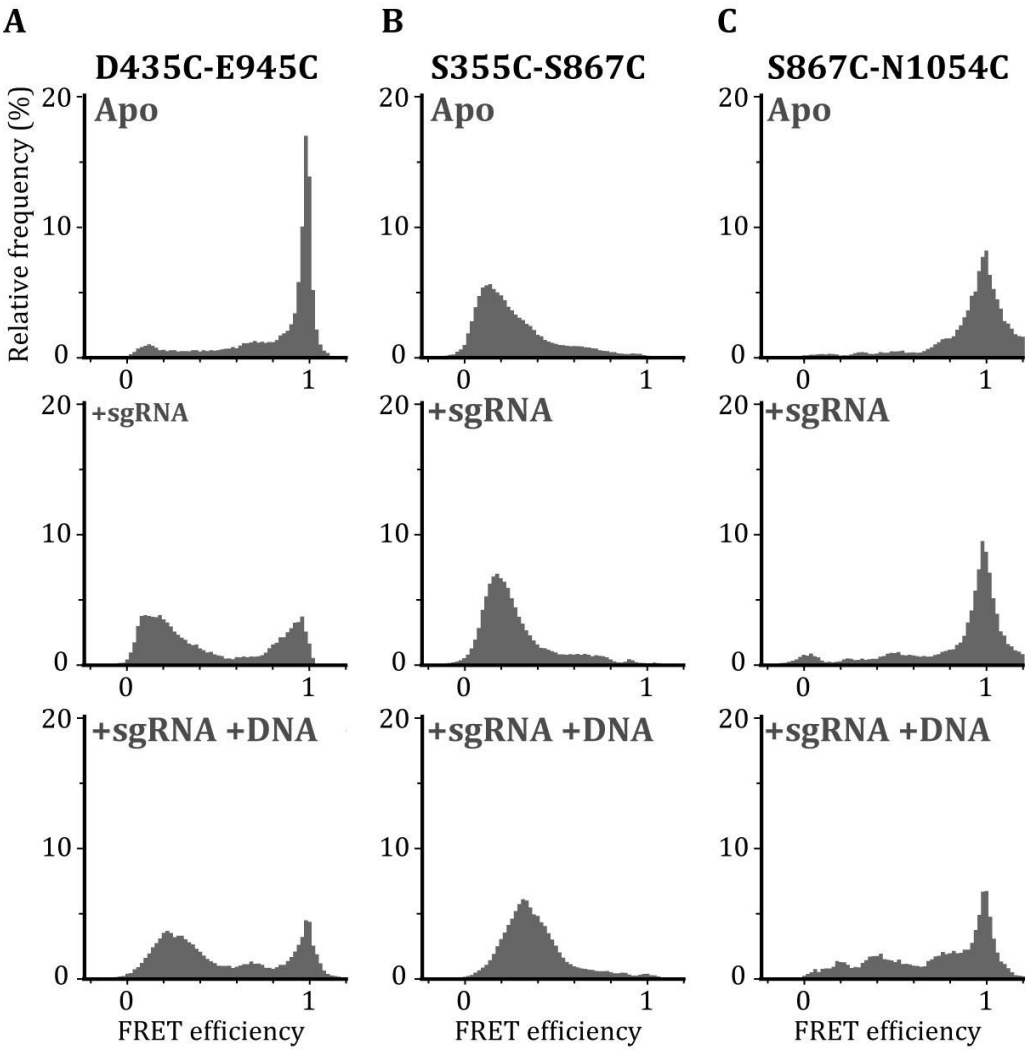


**Figure 2. FRET efficiency histograms of all measured Cas9 molecules.**

(A-C) FRET efficiency histograms of D435C-E945C (A), S355C-S867C (B) and S867C-N1054C (C) constructs. The numbers of measured molecules are summarized in Table EV1. The top, middle and bottom panels show data acquired in the absence of nucleotides, in the presence of 200 nM sgRNA and in the presence of 200 nM sgRNA and 200 nM plasmid DNA, respectively.

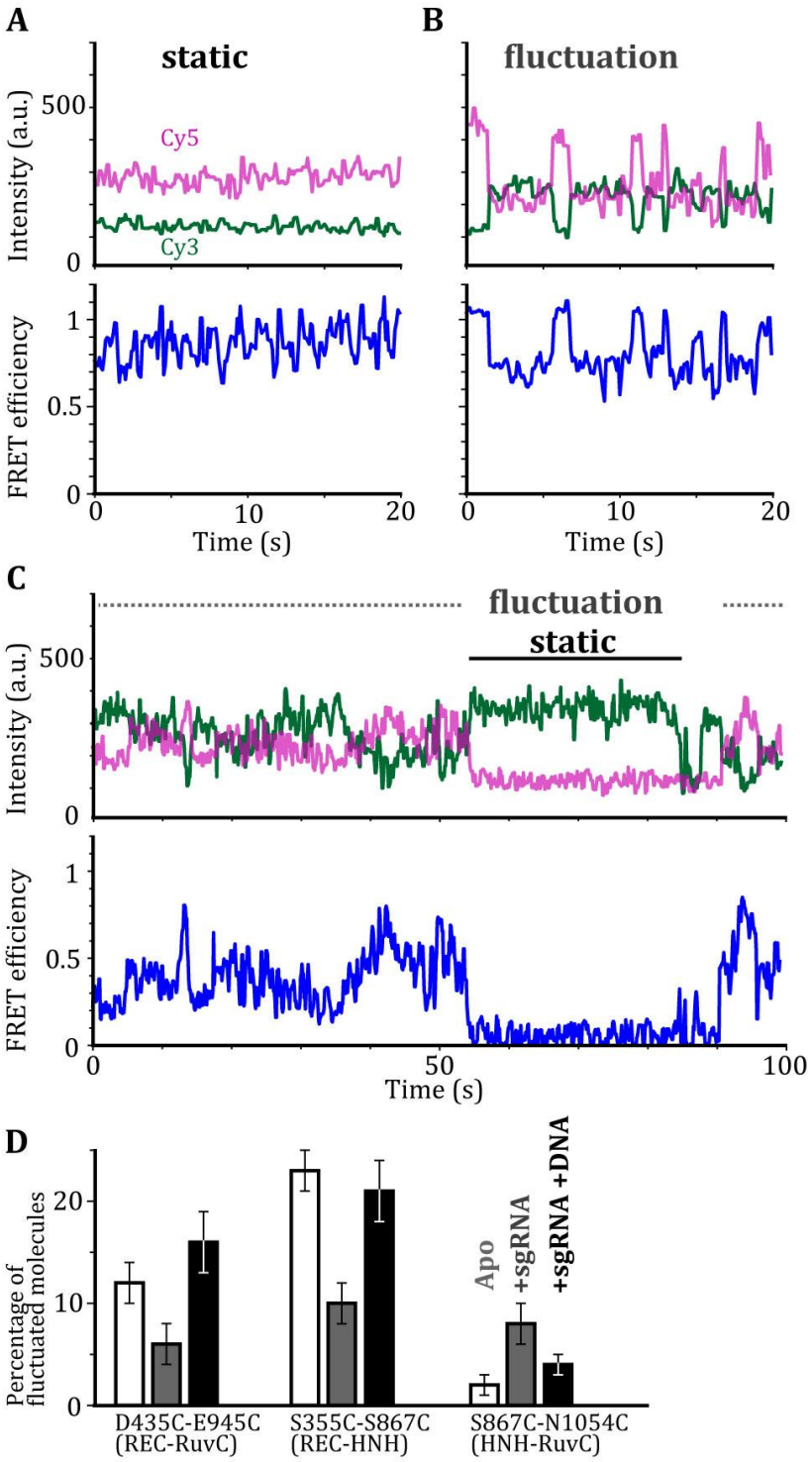


**Figure 3. The binding of sgRNA and target DNA changes flexibility of the Cas9 domains.**

Representative time trajectories showing no fluctuation (A) and fluctuation (B) of

the D435C-E945C construct in the sgRNA/DNA-bound ternary complex labeled with Cy3 and Cy5. The green and magenta lines represent the fluorescence intensities of Cy3 and Cy5, respectively (top trace). We calculated the FRET efficiency (black lines) from the intensities of Cy3 and Cy5 (bottom trace). (C) Some of the time trajectories of the fluorescence intensities (top trace) and single-molecule FRET efficiency (bottom trace) show a static phase and fluctuation phase. (D) The percentage of Cas9 molecules that showed fluctuations in FRET efficiency. The numbers of measured molecules are summarized in Table EV1. The white, gray and black bars represent percentages in the absence of nucleic acid, in the presence of 200 nM sgRNA, and in the presence of 200 nM sgRNA and 200 nM plasmid DNA, respectively. Error bars show SEM.

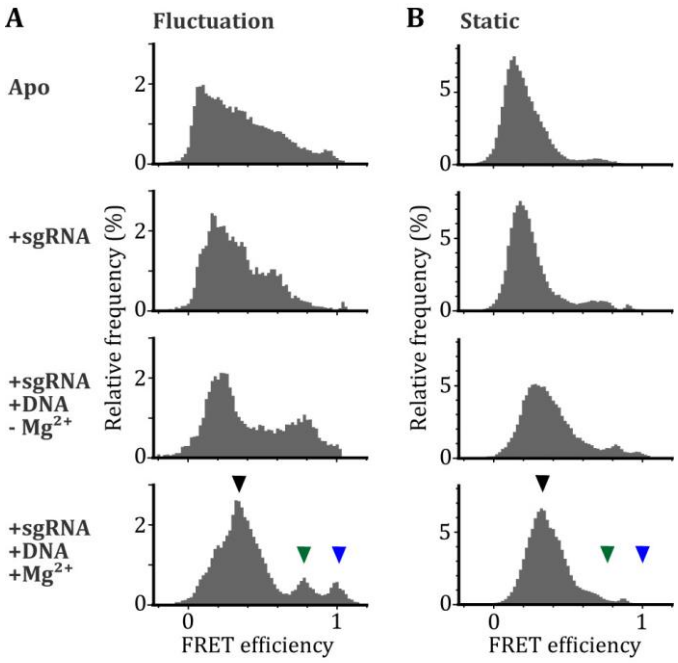


**Figure 4. The HNH domain transiently locates at the DNA-cleavage position during flexible movement.**

(A-B) FRET efficiency histograms of fluctuating (A) and static (B) S355C-S867C molecules. The numbers of measured molecules are summarized in Table EV1. The panels from top to bottom show data in the absence of nucleic acids, in the presence of 200 nM sgRNA, in the presence of 200 nM sgRNA and 200 nM plasmid DNA without $Mg^{2+}$, and in the presence of 200 nM sgRNA and 200 nM plasmid DNA with $Mg^{2+}$, respectively. (A) In the presence of $Mg^{2+}$, the fluctuating molecules exhibited three clear peaks in the FRET efficiency, corresponding to the three HNH positions relative to the REC lobe. According to the structural and functional data, we name the HNH positions corresponding to the low (black arrow head), middle (green arrow head) and high (blue arrow head) FRET efficiency undock, pre-cleavage and DNA-cleavage positions, respectively. The same FRET efficiencies are indicated by the arrow heads in the histogram of static molecules (B).

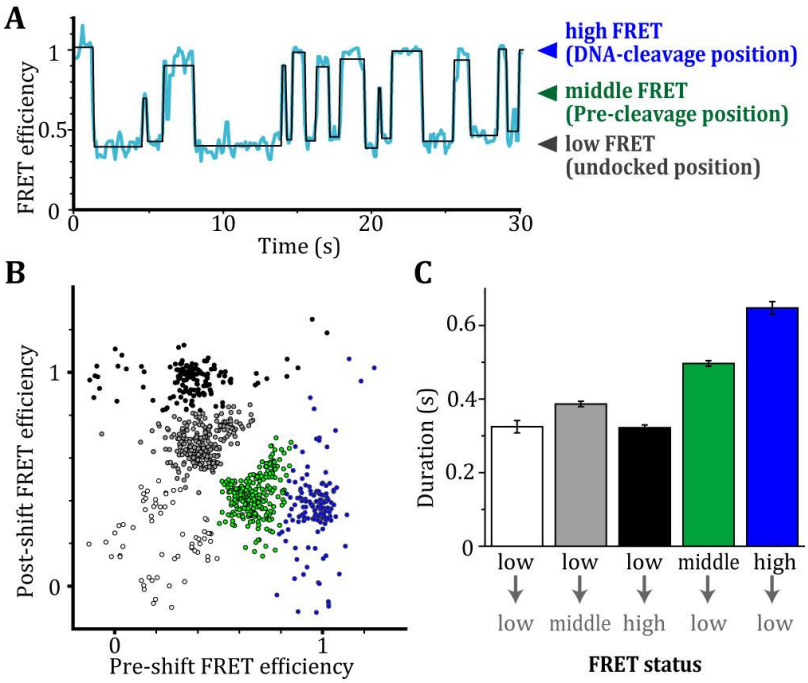


**Figure 5. Reversible transitions in the HNH positioning in the ternary complex.**

(A) Representative time trajectory of FRET efficiency showing fluctuation of the HNH domain in sgRNA/target DNA-bound S355C-S867C with $Mg^{2+}$. The transition points of the FRET efficiency (blue line) were detected using HMM algorithm (black line). (B) The transition density plot of different FRET states of sgRNA/target DNA-bound S355C-S867C with $Mg^{2+}$. The density map was clustered into five groups (white, gray, black, green and blue closed circles) based on the *k*-means method with $k$ = 5, suggesting that HNH movement between the pre-cleavage and DNA-cleavage processes (middle and high FRET efficiency) is rare. (C) Bar plot of the durations for each transition. The mean durations were determined by fitting the duration distributions ($n$ = 56, 219, 124, 223 and 136 for low-low, low-middle, low-high, middle-low and high-low transitions, respectively) to a single exponential decay function. Error bars show SEM.

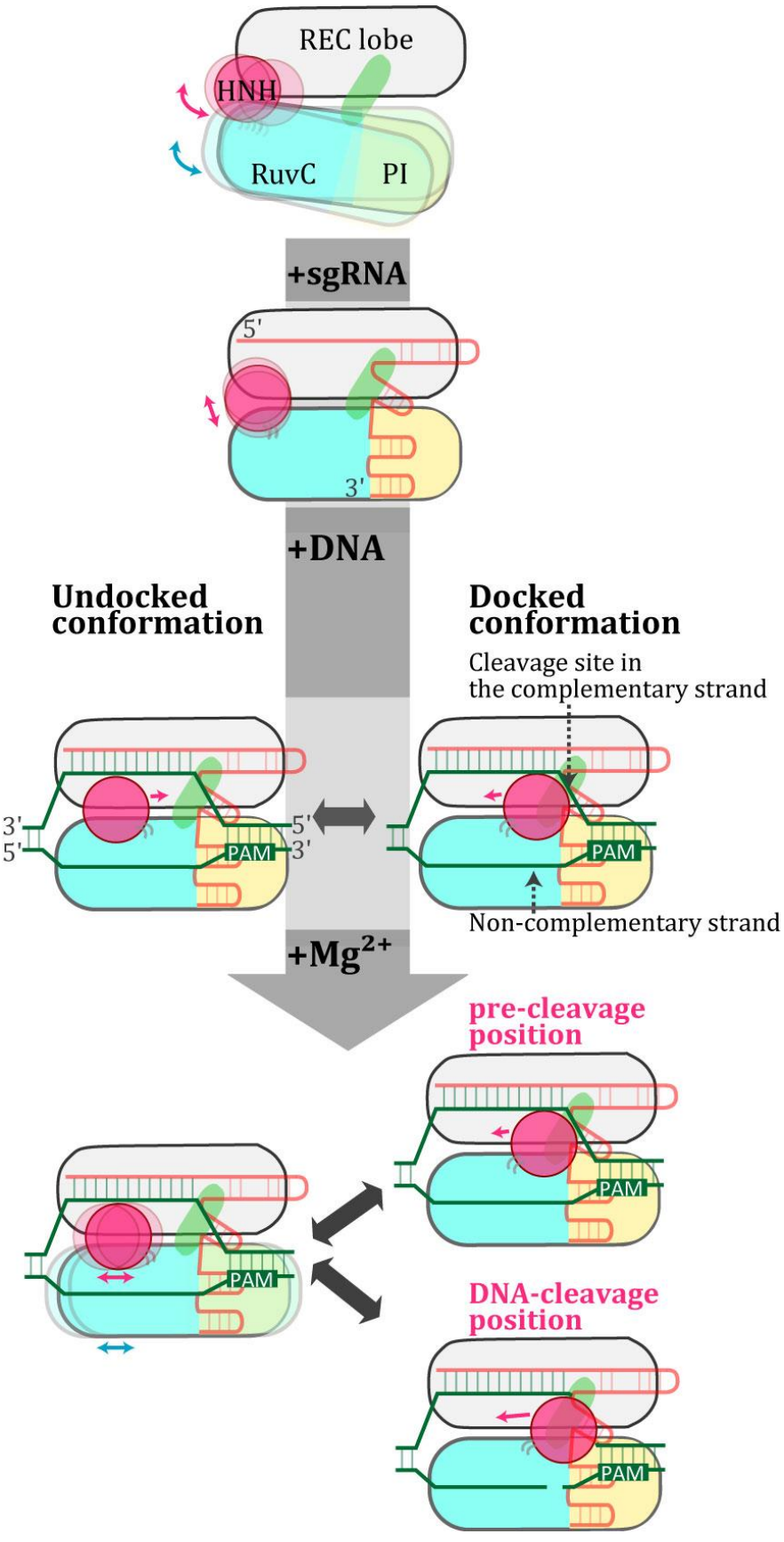

**Figure 6. Model of fluctuations between Cas9 domains during the catalytic processes**

Relative flexible movements of the HNH (magenta) and RuvC (blue) domains against the REC lobe (gray) are represented by the colored arrows. The binding of sgRNA (red) stabilizes the RuvC movements against the REC lobe, but the binding of the target DNA (green) increases the flexibility between the nuclease and REC lobes. The PI domain and the bridge helix in the REC lobe are shown in yellow and green, respectively.

## REFERENCES

Anders C, Niewoehner O, Duerst A & Jinek M (2014) Structural basis of PAM-dependent target DNA recognition by the Cas9 endonuclease. *Nature* **513:** 569–73 Available at: http://www.nature.com/doifinder/10.1038/nature13579%5Cnhttp://www.ncbi.nlm.nih.gov/pubmed/25079318%5Cnhttp://www.ncbi.nlm.nih.gov/pubmed/25079318

Barrangou R, Fremaux C, Deveau H, Richards M, Boyaval P, Moineau S, Romero DA & Horvath P (2007) CRISPR provides acquired resistance against viruses in prokaryotes. *Science* **315:** 1709–12 Available at: http://www.ncbi.nlm.nih.gov/pubmed/17379808

Bolotin A, Quinquis B, Sorokin A & Ehrlich SD (2005) Clustered regularly interspaced short palindrome repeats (CRISPRs) have spacers of extrachromosomal origin. *Microbiology* **151:** 2551–61 Available at: http://www.ncbi.nlm.nih.gov/pubmed/16079334

Cong L, Ran FA, Cox D, Lin S, Barretto R, Habib N, Hsu PD, Wu X, Jiang W, Marraffini LA & Zhang F (2013) Multiplex genome engineering using CRISPR/Cas systems. *Science* **339:** 819–23 Available at: http://www.ncbi.nlm.nih.gov/pubmed/23287718

Dale RE, Eisinger J & Blumberg WE (1979) The orientational freedom of molecular probes. The orientation factor in intramolecular energy transfer. *Biophys. J.* **26:** 161–193 Available at: http://dx.doi.org/10.1016/S0006-3495(79)85243-1

Hsu PD, Lander ES & Zhang F (2014) Development and applications of CRISPR-Cas9 for genome engineering. *Cell* **157:** 1262–1278 Available at: http://dx.doi.org/10.1016/j.cell.2014.05.010

Jansen R, Embden JDA van, Gaastra W & Schouls LM (2002) Identification of genes that are associated with DNA repeats in prokaryotes. *Mol. Microbiol.* **43:** 1565–75 Available at: http://www.ncbi.nlm.nih.gov/pubmed/11952905

Jiang F, Taylor DW, Chen JS, Kornfeld JE, Zhou K, Thompson AJ, Nogales E & Doudna JA (2016) Structures of a CRISPR-Cas9 R-loop complex primed for DNA cleavage. *Science* **351:** 867–71 Available at: http://www.sciencemag.org/cgi/doi/10.1126/science.aad8282

Jiang F, Zhou K, Ma L, Gressel S & Doudna JA (2015) A Cas9-guide RNA complex preorganized for target DNA recognition. *Science* **348:** 1477–1481 Available at: http://eutils.ncbi.nlm.nih.gov/entrez/eutils/elink.fcgi?dbfrom=pubmed&id=26113724&retmode=ref&cmd=prlinks%5Cnpapers2://publication/doi/10.1126/science.aab1452%5Cnhttp://www.sciencemag.org/cgi/doi/10.1126/science.aab1452

Jinek M, Chylinski K, Fonfara I, Hauer M, Doudna JA & Charpentier E (2012) A programmable dual-RNA-guided DNA endonuclease in adaptive bacterial immunity. *Science* **337:** 816–21 Available at: http://www.sciencemag.org/cgi/doi/10.1126/science.1225829

Jinek M, Jiang F, Taylor DW, Sternberg SH, Kaya E, Ma E, Anders C, Hauer M, Zhou K, Lin S, Kaplan M, Iavarone AT, Charpentier E, Nogales E & Doudna JA (2014) Structures of Cas9 endonucleases reveal RNA-mediated conformational activation. *Science* **343:** 1247997 Available at: http://www.pubmedcentral.nih.gov/articlerender.fcgi?artid=4184034&tool=pmcentrez&rendertype=abstract

Kleinstiver BP, Pattanayak V, Prew MS, Tsai SQ, Nguyen NT, Zheng Z & Joung JK (2016) High-fidelity CRISPR–Cas9 nucleases with no detectable genome-wide off-target effects. *Nature* **529:** 490–495 Available at: http://www.nature.com/doifinder/10.1038/nature16526

Konermann S, Brigham MD, Trevino AE, Joung J, Abudayyeh OO, Barcena C, Hsu PD, Habib N, Gootenberg JS, Nishimasu H, Nureki O & Zhang F (2014) Genome-scale transcriptional activation by an engineered CRISPR-Cas9 complex. *Nature* **517:** 583–8 Available at: http://www.pubmedcentral.nih.gov/articlerender.fcgi?artid=4420636&tool=pmcentrez&rendertype=abstract

Mali P, Yang L, Esvelt KM, Aach J, Guell M, DiCarlo JE, Norville JE & Church GM (2013) RNA-guided human genome engineering via Cas9. *Science* **339:** 823–6 Available at: http://www.ncbi.nlm.nih.gov/pubmed/23287722

McKinney SA, Joo C & Ha T (2006) Analysis of single-molecule FRET trajectories using hidden Markov modeling. *Biophys. J.* **91:** 1941–51 Available at: http://www.pubmedcentral.nih.gov/articlerender.fcgi?artid=1544307&tool=pmcentrez&rendertype=abstract [Accessed July 15, 2014]

Mojica FJM, Díez-Villaseñor C, García-Martínez J & Soria E (2005) Intervening sequences of regularly spaced prokaryotic repeats derive from foreign genetic elements. *J. Mol. Evol.* **60:** 174–82 Available at: http://www.ncbi.nlm.nih.gov/pubmed/15791728

Nishimasu H, Ran FA, Hsu PD, Konermann S, Shehata SI, Dohmae N, Ishitani R, Zhang F & Nureki O (2014) Crystal structure of Cas9 in complex with guide RNA and target DNA. *Cell* **156:** 935–949 Available at: http://dx.doi.org/10.1016/j.cell.2014.02.001

Pourcel C, Salvignol G & Vergnaud G (2005) CRISPR elements in Yersinia pestis acquire new repeats by preferential uptake of bacteriophage DNA, and provide additional tools for evolutionary studies. *Microbiology* **151:** 653–63 Available at: http://www.ncbi.nlm.nih.gov/pubmed/15758212

Roy R, Hohng S & Ha T (2008) A practical guide to single-molecule FRET. *Nat. Methods* **5:** 507–516 Available at: http://dx.doi.org/10.1038/nmeth.1208

Shmakov S, Smargon A, Scott D, Cox D, Pyzocha N, Yan W, Abudayyeh OO, Gootenberg JS, Makarova KS, Wolf YI, Severinov K, Zhang F & Koonin E V. (2017) Diversity and evolution of class 2 CRISPR-Cas systems. *Nat. Rev. Microbiol.* **15:** 169–182 Available at: http://www.nature.com/doifinder/10.1038/nrmicro.2016.184

Singh D, Sternberg SH, Fei J, Doudna JA & Ha T (2016) Real-time observation of DNA recognition and rejection by the RNA-guided endonuclease Cas9. *Nat. Commun.* **7:** 12778 Available at: http://www.nature.com/doifinder/10.1038/ncomms12778

Slaymaker IM, Gao L, Zetsche B, Scott DA, Yan WX & Zhang F (2016) Rationally engineered Cas9 nucleases with improved specificity. *Science* **351:** 84–88 Available at: http://www.sciencemag.org/cgi/doi/10.1126/science.aac8608%5Cnhttp://www.sciencemag.org/cgi/doi/10.1126/science.aad5227

Sternberg SH & Doudna JA (2015) Expanding the Biologist's Toolkit with CRISPR-Cas9. *Mol. Cell* **58:** 568–574 Available at: http://dx.doi.org/10.1016/j.molcel.2015.02.032

Sternberg SH, LaFrance B, Kaplan M & Doudna JA (2015) Conformational control of

DNA target cleavage by CRISPR-Cas9. *Nature* **527:** 110–3 Available at: http://www.nature.com/doifinder/10.1038/nature15544

Sternberg SH, Redding S, Jinek M, Greene EC & Doudna JA (2014) DNA interrogation by the CRISPR RNA-guided endonuclease Cas9. *Nature* **507:** 62–7 Available at: http://www.pubmedcentral.nih.gov/articlerender.fcgi?artid=4106473&tool=pmcentrez&rendertype=abstract

Terns RM & Terns MP (2014) CRISPR-based technologies: Prokaryotic defense weapons repurposed. *Trends Genet.* **30:** 111–118 Available at: http://dx.doi.org/10.1016/j.tig.2014.01.003

Zheng W (2017) Probing the structural dynamics of the CRISPR-Cas9 RNA-guided DNA-cleavage system by coarse-grained modeling. *Proteins* **85:** 342–353 Available at: http://www.ncbi.nlm.nih.gov/pubmed/27090373